ACS APPLIED MATERIALS & INTERFACES

Research Article

www.acsami.org

Carbon Quantum Dot/NiFe Layered Double-Hydroxide Composite as a Highly Efficient Electrocatalyst for Water Oxidation

Di Tang, Juan Liu, Xuanyu Wu, Ruihua Liu, Xiao Han, Yuzhi Han, Hui Huang, Yang Liu,* and Zhenhui Kang*

Institute of Functional Nano & Soft Materials (FUNSOM) and Collaborative Innovation Center of Suzhou Nano Science and Technology, Soochow University, Suzhou 215123, China

Supporting Information

ABSTRACT: The design of highly efficient, durable, and earth-abundant catalysts for the oxygen evolution reaction is crucial to a variety of important energy conversion and storage processes. Here, we use carbon quantum dots (CQDs, ~5 nm) to form hybrids with the ultrathin nickel−iron layered double-hydroxide (NiFe-LDH) nanoplates. The resulting CQD/NiFe-LDH complex exhibits high electrocatalytic activity (with an overpotential of ~235 mV in 1 M KOH at a current density of 10 mA cm^{-2}) and stability for oxygen evolution, which almost exceed the values of all previously reported Ni-Fe compounds and were comparable to those of the most active perovskite-based catalyst.

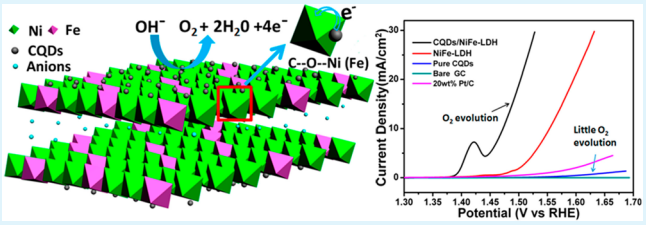

KEYWORDS: *carbon quantum dots, NiFe-LDH complex, enchanced OER, chronopotentiometry, stability*

INTRODUCTION

The electrolysis of water to generate oxygen provides a possible process for the storage of a considerable amount of energy.[1−8] However, the OER (oxygen evolution reaction) is kinetically slow because of its multistep proton-coupled electron transfer process, so electrolysis must require a relatively higher potential than thermodynamic potential (1.23 V) for water splitting ($H_2O \rightarrow H_2 + {}^1/_2O_2$).[9,10] Currently, RuO_2 and IrO_2 are regarded as the most active OER catalysts,[2,11−13] but the lack of Ru and Ir makes it impractical to use the metals on a large scale. Therefore, the development of alternative catalysts that offer an availability suitable for large-scale application and also high efficiency in water electrolysis is critical.

Layered double hydroxides (LDHs), as a family of layered anionic materials, have attracted considerable attention because of their flexible structures and chemical versatility, which have been exploited as a fruitful source of materials for application in electrochemistry, magnetism, catalysis, and chemical sensing.[14−17] In particular, NiFe-LDH possesses a layered and relatively open structure, which makes the rapid diffusion of reactants and products and even the fast proton-coupled electron transfer process in the water oxidation reaction much easier, but the poor electrical conductivity restricts its widespread application in electrocatalysis. Although other carbon-related materials [such as carbon nanotubes (CNTs) and graphene][18−20] have been reported to form composites with LDHs for electrocatalysis applications,[21−23] the complicated design of their functional groups remains a weakness. For instance, Dai et al. reported the integration of a Ni-Fe LDH OER catalyst with mildly oxidized multiwalled CNTs can reduce the external power for a catalyst's electrolysis chemistry (with an overpotential of ~247 mV at 10 mA cm^{-2} in 1 M KOH),[8] but the CNTs they used needed further modification via a modified Hummers method before forming composites with LDHs.

Carbon quantum dots (CQDs), known as a novel class of nanocarbon with abundant functional groups on the surface that are needed for solidly nucleating and anchoring the pristine nanocrystals with CQDs to achieve an intense electrostatic interaction (or covalent attachment), have attracted considerable attention because of their unique physical and chemical properties.[24−28] In particular, their small particle size (~5 nm), up-converted photoluminescence (PL) behavior, supernal conductivity, rapid electron transfer, and electron reservoir properties make it much easier to form composites and thus can further enhance the catalytic activities of the original materials. Previous studies by our group have designed CQD nanocomposite (CQD/$BiVO_4$, CQD/Cu_2O, CQD/Ag_3PO_4, etc.) catalysts, which all showed enhanced photocatalytic properties.[29−32] However, CQD-based nanocomposites as an efficient electrode material for water oxidation have never previously been reported, to the best of our knowledge.

Here, we report the structural and electrochemical investigation of CQD/NiFe-LDH composite catalysts used for the OER in alkaline electrolytes. Via the use of the one-step synthetic CQDs with multifunctional groups to form composites with NiFe-LDH, we can conclude that the CQD/NiFe-LDH composite is a beter OER catalyst than either the

Received: March 1, 2014
Accepted: April 15, 2014
Published: April 15, 2014

   dx.doi.org/10.1021/am501256x | ACS Appl. Mater. Interfaces 2014, 6, 7918−7925

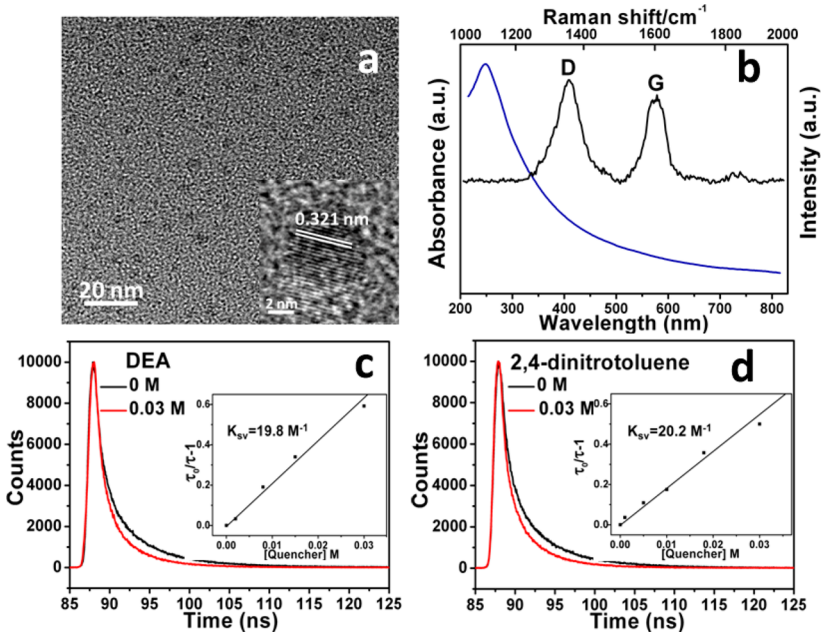

Figure 1. (a) TEM images of the CQDs. The inset in panel a is the HRTEM image of a single CQD particle. (b) UV−vis absorption spectrum (blue) and Raman spectrum (black) of CQDs. Luminescence decays (485 nm excitation, monitored with a 550 nm narrow bandpass filter) of the CQDs with (c) DEA and (d) 2,4-dinitrotoluene. The insets of panels c and d are Stern−Volmer plots for the quenching of luminescence quantum yields of the CQDs by DEA and 2,4-dinitrotoluene, respectively.

pristine NiFe-LDH or the other NiFe composites. That is, the resulting CQD/NiFe-LDH hybrid displays good stability and also excellent OER electrocatalytic activity with a high current and a small overpotential (~235 mV in 1 M KOH and ~305 mV in 0.1 M KOH) at a current density of 10 mA cm^{-2}. This almost exceeded those of any previously reported Ni-Fe compounds[9,11,32,33] and even was comparable to that of the lowest overpotential reported in Ni-Fe catalysts, ~230 mV at 10 mA cm^{-2} for electrodeposited Ni-Fe films.[34]

EXPERIMENTAL SECTION

All chemicals were purchased from Sigma-Aldrich (A.R) and were used as received without further purification.

Preparation of CQDs. CQDs (~5 nm) were synthesized through an electrochemical etching method. In a typical experiment, The graphite rod (99.99%, Alfa Aesar Co. Ltd.) was inserted into the ultrapure water as the anode (18.4 MΩ cm^{-1}, 600 mL), placed parallel to the other graphite rod as the counter electrode with a separation of 7.5 cm. Static potentials of 15−60 V were applied to the two electrodes using a direct current (dc) power supply. After the sample had been continuously stirred for 120 h, the anode graphite rod corroded, and a dark-yellow solution appeared gradually in the reactor. The solution was filtered with slow-speed quantitative filter paper, and the resultant solution was centrifuged at 22000 rpm for 30 min to remove the precipitated graphite oxide and graphite particles. Finally, the obtained solution consisted of water-soluble CQDs.

The ~10 and ~100 nm carbon particles were obtained from gradient centrifugation of the untreated solution by the electrochemical etching method.

Synthesis of the NiFe Hydroxide Carbon Dot Hybrid (CQD/NiFe-LDH). In a typical synthesis, ~2 mg of CQDs was dispersed in 4 mL of anhydrous *N*,*N*-dimethylformamide (DMF), which was aided by sonication for 10 min. After that, 400 μL of 0.2 M nickel acetate [$Ni(OAc)_2$] and 80 μL of a 0.2 M ferrous nitrate [$Fe(NO_3)_3$] aqueous solution were added. The solution was vigorously stirred at 85 °C for 4 h. Then, the product was collected and dispersed in a mixture of ~4 mL of DMF and ~8 mL of water and transferred to a 40 mL Teflon-lined stainless steel autoclave for solvothermal reaction at 120 °C for 12 h, followed by another solvothermal treatment at 160 °C for 2 h. The final product was collected by centrifugation, repetitively washed with water, and lyophilized.

Synthesis of Control Groups of the NiFe-LDH Nanoplate, CQD/β-$Ni(OH)_2$, and CQD/FeOx. All controllable contrast test samples were synthesized by similar procedures of CQD/NiFe-LDH synthesis with different precursors. The NiFe-LDH nanoplate was synthesized with 400 μL of 0.2 M $Ni(OAc)_2$ and 80 μL of a 0.2 M [$Fe(NO_3)_3$] aqueous solution (without a CQD precursor). The CQD/$Ni(OH)_2$ nanoplate hybrid was synthesized with 400 μL of a 0.2 M $Ni(OAc)_2$ aqueous solution and ~2 mg of CQDs [without $Fe(NO_3)_3$ precursors]. The CQD/FeOx composite was synthesized with 400 μL of a 0.2 M $Fe(NO_3)_3$ aqueous solution and ~2 mg of CQDs [without $Ni(OAc)_2$ precursors]. All hybrid materials contain ~18.5 wt % CQDs.

RESULTS AND DISCUSSION

In our experiments, high-purity CQDs were synthesized through a mild, one-step electrochemical approach, without the assistance of any chemicals but only pure water.[40] The gained CQDs possess fragmented graphitic structure and abundent functional groups on the surface without further modification. Figure 1a shows the transmission electron microscopy (TEM) image of CQDs, revealing that the diameter of CQDs is ~5 nm. The high-resolution TEM (HRTEM) image in the inset of Figure 1a depicts the crystal lattice spacing of ~0.321 nm, which agrees well with the (002) lattice planes of graphitic carbon. The UV−vis absorption spectrum of CQDs (in Figure 1b, blue curve) typically shows an obvious optical absorption peak in 260 nm, with a tail extending to the visible range, and there are also two characteristic peaks located at ~1358 and ~1600 cm^{-1} in the Raman spectrum of CQDs (in Figure 1b, black curve), corresponding to the D-band and G-band of carbon, respectively. Panels c and d of Figure 1 display the luminescence decays (485 nm excitation, monitored with a 550 nm narrow bandpass filter) of CQDs, which were quenched by given electron donor *N*,*N*-diethylaniline (DEA,

dx.doi.org/10.1021/am501256x | ACS Appl. Mater. Interfaces 2014, 6, 7918−7925

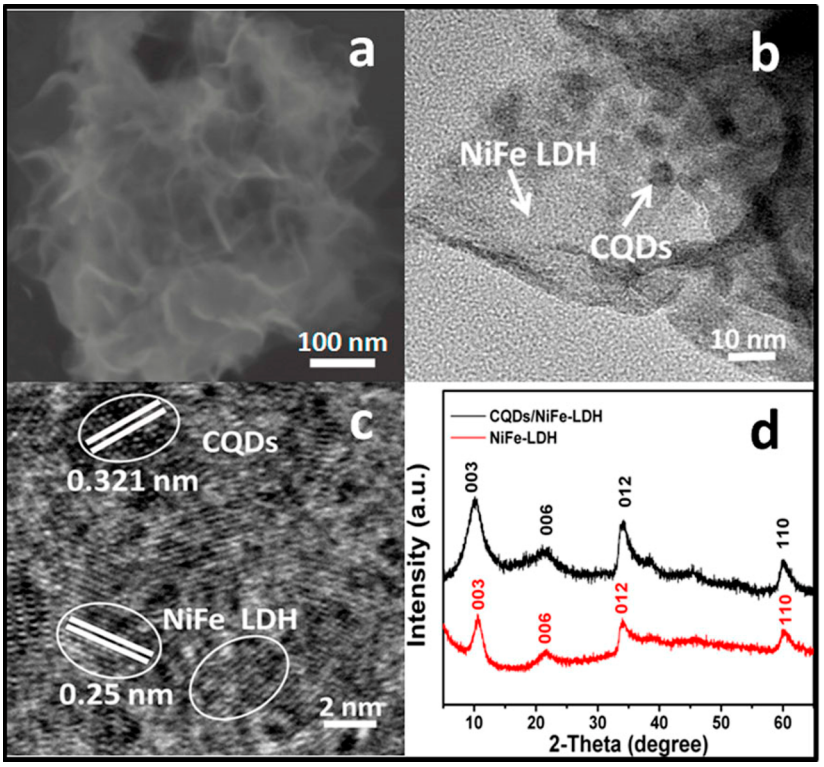

Figure 2. (a) SEM image of the CQD/NiFe-LDH nanoplate catalyst. (b) TEM and (c) HRTEM images of the CQD/NiFe-LDH hybrid. Arrows point to individual NiFe-LDH plates and smaller CQD particles. (d) XRD spectra of the CQD/NiFe-LDH (black) and pure NiFe-LDH (red, synthesized without CQDs) samples.

0.88 V vs NHE) and electron acceptor 2,4-dinitrotoluene (−0.9 V vs NHE), with the observed Stern−Volmer (insets of panels c and d of Figure 1) quenching constants ($K_{SV} = \tau F^{\circ} kq$) from linear regression of 19.8 and 20.2 M^{-1}, respectively. The distinct results that show that the PL spectra of CQDs were quenched highly efficiently by either electron acceptors or electron donors clearly demonstrate that CQDs are prominent as both electron donors and electron acceptors.[31]

In our experiments, a facile method was developed to synthesize the CQD/NiFe-LDH composite.[8] Typically, nickel acetate and iron nitrate (with a Ni/Fe molar ratio of 5) were hydrolyzed in a mixed *N*,*N*-dimethylformamide (DMF) and CQD aqueous solution at 85 °C for 4 h. Followed by redispersion of the intermediate product in a DMF/H_2O mixed solvent and through a solvothermal treatment at 120 °C for 12 h was a second solvothermal step at 160 °C for 2 h. The solvothermal treatment may lead to the crystallization of NiFe-LDH nanoplates and the formation of the nanocomposites.

The structure, size, and morphology of the fabricated hybrid were characterized by scanning electron microscopy (SEM) and TEM. Figure 2a shows the SEM images of the CQD/NiFe-LDH composite. It shows that the nanoplates are ultrathin [~1 nm (see the AFM image in Figure S1 of the Supporting Information for details)] and have a variable size of approximately 50−200 nm. The TEM image (see Figure 2b) shows that the NiFe-LDH nanoplate and CQDs (size of ~5 nm) successfully formed a composite. The HRTEM (Figure 2c) image of the CQD/NiFe-LDH composite further reveals that the fringe spacing of 0.25 nm agrees well with the spacing of the (012) lattice plane of NiFe-LDH, while the interplanar spacing of ~0.321 nm corresponds to the (002) crystallographic planes of graphitic carbon, which is strong evidence of the formation of CQD/NiFe-LDH composite structures. Energy-dispersive X-ray spectrum (EDS) analysis (shown in Figure S2 of the Supporting Information) also suggested the formation of the stoichiometric NiFe-LDH compound and the related complex photocatalysts. It is easy to see that, in addition to the Ni, Fe, and O stemming from the pristine NiFe-LDH, the C peaks corresponding to CQDs (CQD content of ~18.5%) can be distinctly detected in the CQD/NiFe-LDH composite catalysts. Figure 2d shows X-ray diffraction (XRD) patterns of the as-prepared CQD/NiFe-LDH electrocatalyst, which is in good agreement with the standard data of α-$Ni(OH)_2$ (the same structure as NiFe-LDH)[8] (JCPDS Card 38-0715). No extra characteristic peaks were detected from the patterns, indicating that there were no impurities in the products. The characteristic peak for carbon at 26° is too weak to be observed, perhaps because of the small amount of carbon and its relatively low diffraction intensity in composites. It is known that incorporation of Fe^{3+} into nickel hydroxide could replace Ni^{2+} in the $Ni(OH)_2$ lattice, thus forming a stable LDH structure. The excessive cationic charge caused by Fe^{3+} was balanced by intercalation of the anion between the hydroxide layers.[35−38] From the X-ray photoelectron spectroscopy (XPS) image shown in Figure S3 of the Supporting Information, the existence of both Fe and Ni in the hybrid material was proven, and the Fe species was confirmed to be mostly in the +3 oxidation state from the high-resolution Fe 2p spectrum (see Figure S3b of the Supporting Information).

In the subsequent experiments, we further investigated the interaction between the CQDs and NiFe-LDH components in the hybrid catalyst. The FT-IR spectra of CQDs and the CQD/NiFe-LDH composite are displayed in Figure 3a. With respect to pure CQDs, there are several peaks located at approximately

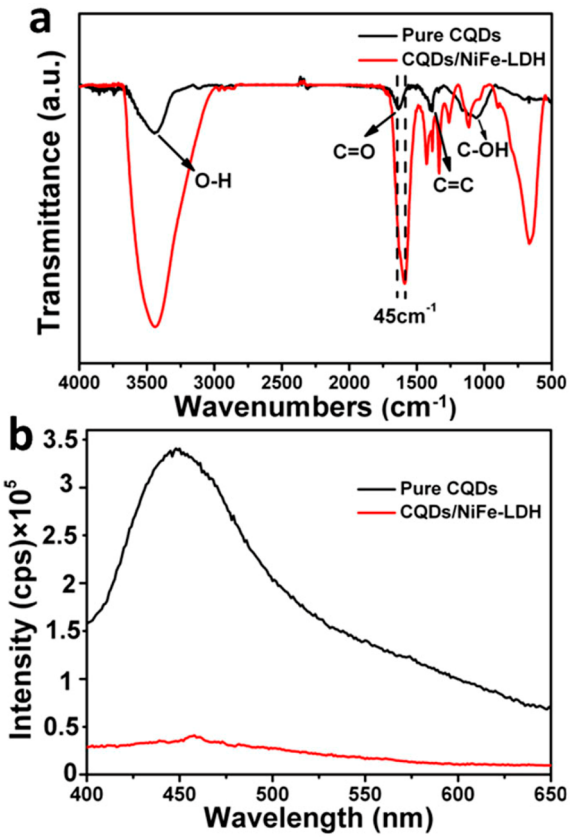

Figure 3. (a) FT-IR and (b) PL spectra of pure CQDs alone and the CQD/NiFe-LDH composite.

3482 (hydroxyl, OH), 1708 (carboxy, C═O), 1440 (aromatic, C═C), and 1243.79 (C−O−H) cm^{-1}. Some peaks for CQDs correspond to the oxygen-containing groups and other new functional groups, indicating a successful oxidation of graphite and the formation of hydrophilic groups. Compared with pure CQDs, the CQD/NiFe-LDH composite shows a slight shift of some dominant peaks [for example, the C═O peak shifts ∼45 cm^{-1} (see the enlarged image in Figure S4 of the Supporting Information)]; this is probably due to the strong electrostatic interactions between NiFe-LDH and CQDs [or the formation of a C−O−M (M represents Ni or Fe here) species that is chemically bound]. This crucial result demonstrates that CQDs here do not just exhibit physical absorption with NiFe-LDH; they also have additional strong interactions with the pristine materials. Figure 3b further shows the PL spectra of CQDs and CQD/NiFe-LDH composite catalysts. We know from panels c and d of Figure 1 that the PL from CQDs can be quenched efficiently by either electron acceptor or electron donor molecules in solution; in particular, CQDs are both excellent electron donors and electron acceptors.[24] From the remarkable decay (or quenching) of PL intensity in the CQD/NiFe-LDH composite compared with that of pure CQDs in Figure 3b, we can conclude that there should have been electron transfers from CQDs to NiFe-LDH nanoplates.

To assess the catalytic properties of the new as-prepared CQD/NiFe-LDH composites for electrochemical oxidation of water to oxygen, the complexes were prepared on glassy carbon electrodes for recording OER polarization curves at a slow scan rate of 5 mV/s in 1 M KOH. During the measurements, the working electrode was continuously rotating at 1600 rpm to remove the generated oxygen bubbles. Similar measurements for the NiFe-LDH nanoplate, a commercial Pt/C reference (Johnson-Matthey, 20 wt %), pure CQDs, and a bare glassy carbon (GC) electrode were also performed. As shown in Figure 4, we can see that the CQD/NiFe-LDH composite

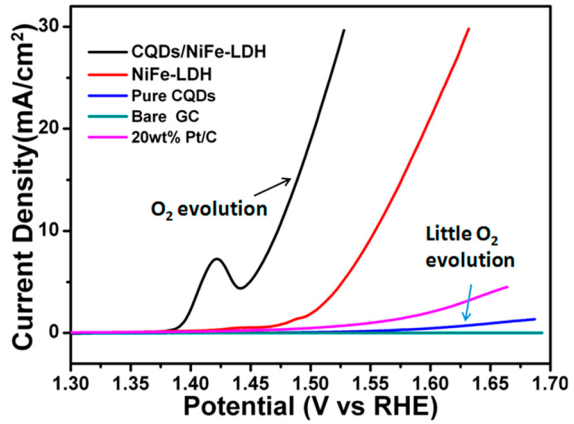

Figure 4. Polarization curves for OER in 1 M KOH on a bare GC electrode and modified GC electrodes comprising pure CQDs, 20 wt % Pt/C, pure NiFe-LDH NPs, and CQD/NiFe-LDH.

(carbon size of ∼5 nm) exhibits the greatest current and earliest onset potential [∼1.44 V vs the reversible hydrogen electrode (RHE)] compared with those of the pure NiFe-LDH composite and other materials. Therefore, we can infer that CQDs definitely play an irreplaceable role in the dramatic enhancement of OER activities in CQD/NiFe-LDH hybrids. It is of note that the free NiFe-LDH composite nanoplates synthesized without CQDs also represent a relatively high OER activity.

Figure 4 suggests that the CQD/NiFe-LDH composite was a novel electrocatalyst material with high OER activity in basic solutions, and we deduce that the strong electrocatalytic performance is mainly attributed to the formation of the NiFe-LDH phase. Strong association of the LDH with CQDs further facilitated charge transport and improved catalyst activity. Therefore, in our further studies, a series of control experiments were conducted to prove the hypothesis. In Figure 5, we can see that CQD/FeO_x, CQD/β-$Ni(OH)_2$, and a physical mixture of them all show a relatively low OER activity compared with that of the pure NiFe-LDH phase, not to mention the CQD/NiFe-LDH hybrid. In 0.1 M KOH, the CQD/NiFe-LDH catalyst showed an onset potential of OER at ∼1.49 V versus the RHE, along with a sharp anodic current (Figure 5a). Similarly, the OER onset potential of the composite is considerably reduced to ∼1.44 V versus the RHE in 1 M KOH (Figure 5b). The prior peak of CQD/NiFe-LDH around 1.43 V in 1 M KOH is assigned to the Ni(II)/Ni(III or IV) redox process.[34] The CQD/NiFe-LDH electrocatalyst was among the most active non-precious metal electrocatalysts.[7,8,11,13,38,39]

In our subsequent experiments, the stability of the CQD/NiFe-LDH composite was also studied on a rotating disk electrode in alkaline solutions at a constant current density of 2.5 mA/cm^2. From Figure 6a, we can see that the CQD/NiFe-LDH composite catalyst had a nearly constant operating potential, at ∼1.51 V (corresponding to an overpotential of 0.28 V) in 0.1 M KOH, whereas the pristine NiFe-LDH composite showed a phanic increase in overpotential of ∼20 mV in 3000 s. Analogously, in 1 M KOH, the working potential

dx.doi.org/10.1021/am501256x | ACS Appl. Mater. Interfaces 2014, 6, 7918−7925

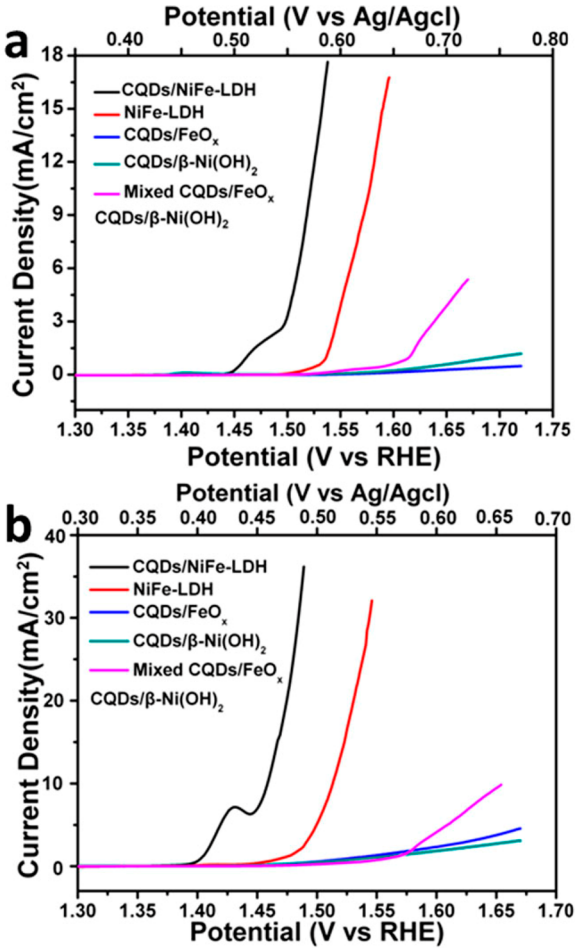

Figure 5. IR-corrected polarization curves of the CQD/NiFe-LDH composite, the NiFe-LDH nanoplate alone, β-Ni(OH)$_2$/CQD nanoparticles, FeO$_x$/CQD nanoparticles, and a physical mixture of β-Ni(OH)$_2$/CQD nanoparticles with FeO$_x$/CQD nanoparticles loaded on the GC electrode (with a loading of 0.2 mg/cm^2) in (a) 0.1 M KOH and (b) 1 M KOH.

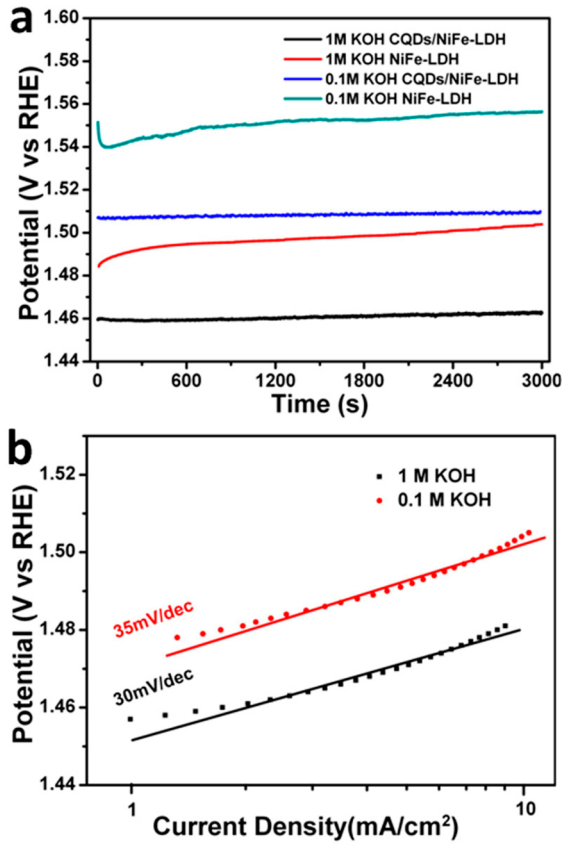

Figure 6. (a) Chronopotentiometry curves of the CQD/NiFe-LDH composite and the pure NiFe-LDH nanoplate catalyst on the GC electrode at a constant current density of 2.5 mA/cm^2 in 0.1 and 1 M KOH. (b) Tafel plots (overpotential vs log current) of the CQD/NiFe-LDH catalyst recorded at a sweep rate of 0.1 mV/s in 0.1 and 1 M KOH.

of the CQD/NiFe-LDH composite was lowered to ∼1.46 V, and the catalyst was also more stable than the pure form. Thus, we can conclude that besides excellect OER activity, the CQD/NiFe-LDH composite electrocatalyst also exhibits good durability in basic solutions. Steady-state Tafel measurements for the CQD/NiFe-LDH composite are presented in Figure 6b. All tafel slopes were fit to the linear region of the data below 1 mA cm^{-2}. The CQD/NiFe-LDH composite catalyst exhibited a Tafel slope of ≈35 mV/decade in 0.1 M KOH and ≈30 mV/decade in 1 M KOH, which are lower than that of pure NiFe-LDH nanoplates and previously reported Ni(Fe)-based OER catalysts under the same conditions.[8,9,11] Moreover, we also examined the SEM images and XRD patterns of the CQD/NiFe-LDH composite catalysts after the long OER operation (see panels a and b of Figure S5 of the Supporting Information). The morphology and size of the NiFe-LDH nanoplate remained the same, and the XRD pattern was consistent with the pristine crystalline NiFe-LDH phase, suggesting no change in the LDH phase through OER catalysis. Thus, we may summarize that highly OER active, relatively stable crystalline CQD/NiFe-LDH nanocomposites in basic solutions have been successfully synthesized.

On the basis of the results and discussions presented above, the proposed mechanism for the excellent OER electrochemical activity of CQD/NiFe-LDH nanocomposites is represented in Figure 7. The high electrocatalytic property was primarily attributed to the NiFe-LDH phase and further enhanced by strong association of the LDH with CQDs, which are small and exhibit excellent conductivity, rapid electron transfer, and electron reservoir properties. Specifically, the small size of CQDs may provide a large specific surface area for more convenient electrocatalytic reaction, and the rapid electron

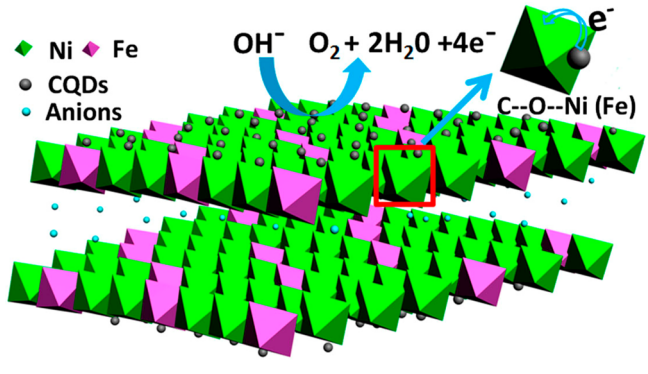

Figure 7. Schematic model of the roles of CQDs in the high elecotrocatalytic activity of CQD/NiFe-LDH nanocomposites.

transfers from CQDs to NiFe-LDH on the surface could further improve the electrocatalytic activities. The surface functional groups on CQDs (such as carboxy C═O) make the formation of CQD/NiFe-LDH composites easier because of the strong electrostatic interactions between NiFe-LDH and CQDs [or generation of a new covalent bond (like C−O−Ni or C−O−Fe)]. Regardless, the synergistic effect between NiFe-LDH and CQDs afforded by direct integration of the Ni−Fe LDH nanoplates with the surface functional groups on CQDs contributed to the optimal OER activity of the CQD/NiFe-LDH composite catalysts.

On the basis of the results presented above, we can see that the CQDs can significantly increase the electrocatalytic activities and durability of NiFe-LDH because of the bonding and interaction between the CQDs and the pure NiFe-LDH nanoplate. As further confirmation that the excellent catalytic properties of the hybrids for water oxidation were attributed to the CQDs rather than random carbon materials, we employed three different sizes of nanocarbon [(a) ∼5 nm, namely CQDs, (b) ∼10 nm, and (c) ∼100 nm] to form composites with NiFe-LDH under the same conditions for comparison. Each of the as-prepared complexes was prepared on a glassy carbon electrode for recording OER polarization curves at a slow scan rate of 5 mV/s in 1 M KOH. Figure 8 shows that with the

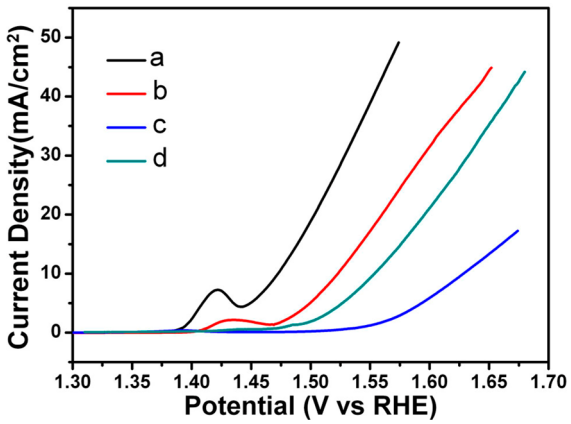

Figure 8. Three different sizes of nanocarbon [(a) ∼5, (b) ∼10, and (c) ∼100 nm] for forming composites with NiFe-LDH as electrocatalysts for OER in 1 M KOH. Trace d is that of NiFe-LDH alone.

increase in the size of nanocarbon, the electrocatalytic activities of the composites decrease apparently. In proper terms, the CQD/NiFe-LDH composite exhibits the greatest current and earliest onset potential (∼1.44 V vs the RHE); ∼10 nm carbon with NiFe-LDH composites has an onset potential of ∼1.47 V, and the value for ∼100 nm carbon decreases to ∼1.55 V, which is even lower than that of the bare NiFe-LDH nanoplate. Therefore, we can conclude that it is definitely CQDs that cooperate with NiFe-LDH to enhance the electrocatalytic OER activities drastically.

It should be further pointed out that, in the system presented here, CQDs with abundant functional groups and unique physicochemical properties are much easier to design than some other nanocarbon materials that might need further modification before being used. Although possessing excellent electrocatalytic properties, the CQD/NiFe-LDH composite presented here still has the benefit that it can be further optimized by introduction of different nanostructures (nanowires, -tubes, -rods, and -plates or their arrays) and different kinds of LDHs (Zn-Co, Ni-Al, Zn-Cr, etc.). Further, CQDs with proper surface modifications, as well as doping with nonmetals, such as N, B, P, and S, might also improve the electrocatalytic performance.[41,42] Given the diversity and versatility of the structural design of the CQD/NiFe-LDH composite system presented here, the combination of CQDs and NiFe-LDH nanoplates as a superb electrocatalyst may provide a new approach to high-efficiency CQD-related electrocatalyst design for applications toward new energy sources, green chemistry, and environmental issues.

CONCLUSIONS

In summary, we report that an advanced CQD/NiFe-LDH nanocomposite catalyst can be synthesized by a plain coprecipitation−solvothermal route. This inexpensive, earth-abundant, and easily constructed catalyst exhibited excellent OER electrochemical activity with small overpotentials of ∼235 mV in 1 M KOH and ∼305 mV in 0.1 M KOH at a current density of 10 mA cm^{-2} and large anodic currents in an alkaline medium. Furthermore, the chronopotentiometry tests with the CQD/NiFe-LDH composite catalyst revealed its good durability. Our studies provide new insight into designing and fabricating effective OER electrocatalysts by synergistic coupling of nonprecious functional materials with CQDs, which are strongly required for energy conversion and storage technologies.

ASSOCIATED CONTENT

Supporting Information

AFM images and EDX, Raman, and XPS spectra of the CQD/NiFe-LDH composites. This material is available free of charge via the Internet at http://pubs.acs.org.

AUTHOR INFORMATION

Corresponding Authors

*E-mail: zhkang@suda.edu.cn.
*E-mail: yangl@suda.edu.cn.

Notes

The authors declare no competing financial interest.

ACKNOWLEDGMENTS

This work was supported by the National Basic Research Program of China (973 Program) (2012CB825800 and 2013CB932702), the National Natural Science Foundation of China (51132006, 21073127, and 21071104), the Specialized Research Fund for the Doctoral Program of Higher Education (20123201110018), a Suzhou Planning Project of Science and Technology (ZXG2012028), a Foundation for the Author of National Excellent Doctoral Dissertation of China (200929), and a project funded by the Priority Academic Program Development of Jiansu Higher Education Institutions.

REFERENCES

(1) Kanan, M. W.; Nocera, D. G. In Situ Formation of an Oxygen-Evolving Catalyst in Neutral Water Containing Phosphate and Co^{2+}. *Science* **2008**, *321*, 1072−1075.

(2) Walter, M. G.; Warren, E. L.; McKone, J. R.; Boettcher, S. W.; Mi, Q.; Santori, E. A.; Lewis, N. S. Solar Water Splitting Cells. *Chem. Rev.* **2010**, *110*, 6446−6473.

(3) Kwon, G.; Ferguson, G. A.; Heard, C. J.; Tyo, E. C.; Yin, C.; DeBartolo, J.; Seifert, S.; Winans, R. E.; Kropf, A. J.; Greeley, J.; Johnston, R. L.; Curtiss, L. A.; Pellin, M. J.; Vajda, S. Size-Dependent

Subnanometer Pd Cluster (Pd_4, Pd_6, and Pd_{17}) Water Oxidation Electrocatalysis. *ACS Nano* **2013**, *7*, 5808−5817.
(4) Pertykin, V.; Macounova, K.; Shlyakhtin, O. A.; Krtil, P. Tailoring the Selectivity for Electrocatalytic Oxygen Evolution on Ruthenium Oxides by Zinc Substitution. *Angew. Chem., Int. Ed.* **2010**, *49*, 4813−4815.
(5) Zhou, W.; Wu, X.-J.; Cao, X.; Huang, X.; Tan, C.; Tian, J.; Liu, H.; Wang, J.; Zhang, H. Ni_3S_2 nanorods/Ni foam Composite Electrode with Low Overpotential for Electrocatalytic Oxygen Evolution. *Energy Environ. Sci.* **2013**, *6*, 2921−2924.
(6) Bergmann, A.; Zaharieva, I.; Dau, H.; Strasser, P. Electrochemical Water Splitting by Layered and 3D Crosslinked Manganese Oxides: Correlating Structural Motifs and Catalytic Activity. *Energy Environ. Sci.* **2013**, *6*, 2745−2755.
(7) Gao, M.-R.; Xu, Y.-F.; Jiang, J.; Zheng, Y.-R.; Yu, S.-H. Water Oxidation Electrocatalyzed by an Efficient $Mn_3O_4/CoSe_2$ Nanocomposite. *J. Am. Chem. Soc.* **2012**, *134*, 2930−2933.
(8) Gong, M.; Li, Y.; Wang, H.; Liang, Y.; Wu, J. Z.; Zhou, J.; Wang, J.; Regier, T.; Wei, F.; Dai, H. An Advanced Ni-Fe Layered Double Hydroxide Electrocatalyst for Water Oxidation. *J. Am. Chem. Soc.* **2013**, *135*, 8452−8455.
(9) Louie, M. W.; Bell, A. T. An Investigation of Thin-Film Ni-Fe Oxide Catalysts for the Electrochemical Evolution of Oxygen. *J. Am. Chem. Soc.* **2013**, *135*, 12329−12337.
(10) Koper, M. T. M. Thermodynamic Theory of Multi-electron Transfer Reactions: Implications for Electrocatalysis. *J. Electroanal. Chem.* **2011**, *660*, 254−260.
(11) Trotochaud, L.; Ranney, J. K.; Williams, K. N.; Boettcher, S. W. Solution-Cast Metal Oxide Thin Film Electrocatalysts for Oxygen Evolution. *J. Am. Chem. Soc.* **2012**, *134*, 17253−17261.
(12) Lee, Y.; Suntivich, J.; May, K. J.; Perry, E. E.; Shao-Horn, Y. Synthesis and Activities of Rutile IrO_2 and RuO_2 Nanoparticles for Oxygen Evolution in Acid and Alkaline Solutions. *J. Phys. Chem. Lett.* **2012**, *3*, 399−404.
(13) Fekete, M.; Hocking, R. K.; Chang, S. L. Y.; Italiano, C.; Patti, A. F.; Arena, F.; Spiccia, L. Highly Active Screen-printed Electrocatalysts for Water Oxidation Based on β-Manganese Oxide. *Energy Environ. Sci.* **2013**, *6*, 2222−2232.
(14) Abellán, G.; Coronado, E.; Martí-Gastaldo, C.; Pinilla-Cienfuegos, E.; Ribera, A. Hexagonal Nanosheets from the Exfoliation of Ni^{2+}-Fe^{3+} LDHs: A Route Towards Layered Multifunctional Materials. *J. Mater. Chem.* **2010**, *20*, 7451−7455.
(15) Evans, D. G.; Duan, X. Preparation of Layered Double Hydroxides and their Applications as Additives in Polymers, as Precursors to Magnetic Materials and in Biology and Medicine. *Chem. Commun.* **2006**, 485−496.
(16) Caravaggio, G. A.; Detellier, C.; Wronski, Z. Synthesis, Stability and Electrochemical Properties of NiAl and NiV Layered Double Hydroxides. *J. Mater. Chem.* **2001**, *11*, 912−921.
(17) Abellán, G.; Busolo, F.; Coronado, E.; Martí-Gastaldo, C.; Ribera, A. Hybrid Magnetic Multilayers by Intercalation of Cu(II) Phthalocyanine in LDH Hosts. *J. Phys. Chem. C* **2012**, *116*, 15756−15764.
(18) Compton, O. C.; Nguyen, S. T. Graphene Oxide, Highly Reduced Graphene Oxide, and Graphene: Versatile Building Blocks for Carbon-Based Materials. *Small* **2010**, *6*, 711−723.
(19) Zhang, Y.; Zhang, N.; Tang, Z.-R.; Xu, Y.-J. Graphene Transforms Wide Band Gap ZnS to a Visible Light Photocatalyst. The New Role of Graphene as a Macromolecular Photosensitizer. *ACS Nano* **2012**, *6*, 9777−9789.
(20) Huang, X.; Yin, Z.; Wu, S.; Qi, X.; He, Q.; Zhang, Q.; Yan, Q.; Boey, F.; Zhang, H. Graphene-Based Materials: Synthesis, Characterization, Properties, and Applications. *Small* **2011**, *7*, 1876−1902.
(21) Wang, H.; Xiang, X.; Li, F. Facile Synthesis and Novel Electrocatalytic Performance of Nanostructured Ni−Al Layered Double Hydroxide/Carbon Nanotube Composites. *J. Mater. Chem.* **2010**, *20*, 3944−3952.
(22) Zhang, L.; Wang, J.; Zhu, J.; Zhang, X.; Hui, K. S.; Hui, K. N. 3D Porous Layered Double Hydroxides Grown on Graphene as Advanced Electrochemical Pseudocapacitor Materials. *J. Mater. Chem. A* **2013**, *1*, 9046−9053.
(23) Li, M.; Zhu, J. E.; Zhang, L.; Chen, X.; Zhang, H.; Zhang, F.; Xu, S.; Evans, D. G. Facile Synthesis of NiAl-Layered Double Hydroxide/Graphene Hybrid with Enhanced Electrochemical Properties for Detection of Dopamine. *Nanoscale* **2011**, *3*, 4240−4246.
(24) Li, H.; Kang, Z.; Liu, Y.; Lee, S.-T. Carbon Nanodots: Synthesis, Properties and Applications. *J. Mater. Chem.* **2012**, *22*, 24230−24253.
(25) Sun, Y.-P.; Zhou, B.; Lin, Y.; Wang, W.; Fernando, K. A. S.; Pathak, P.; Meziani, M. J.; Harruff, B. A.; Wang, X.; Wang, H.; Luo, P. G.; Yang, H.; Kose, M. E.; Chen, B.; Veca, L. M.; Xie, S.-Y. Quantum-Sized Carbon Dots for Bright and Colorful Photoluminescence. *J. Am. Chem. Soc.* **2006**, *128*, 7756−7757.
(26) Li, H. T.; He, X. D.; Kang, Z. H.; Huang, H.; Liu, Y.; Liu, J. L.; Lian, S. Y.; Tsang, C. H. A.; Yang, X. B.; Lee, S.-T. Water-Soluble Fluorescent Carbon Quantum Dots and Photocatalyst Design. *Angew. Chem., Int. Ed.* **2010**, *49*, 4430−4434.
(27) Ma, Z.; Zhang, Y.-L.; Wang, L.; Ming, H.; Li, H.; Zhang, X.; Wang, F.; Liu, Y.; Kang, Z.; Lee, S.-T. Bioinspired Photoelectric Conversion System Based on Carbon-Quantum-Dot-Doped Dye-Semiconductor Complex. *ACS Appl. Mater. Interfaces* **2013**, *5*, 5080−5084.
(28) Baker, S. N.; Baker, G. A. Luminescent Carbon Nanodots: Emergent Nanolights. *Angew. Chem., Int. Ed.* **2010**, *49*, 6726−6744.
(29) Tang, D.; Zhang, H.; Huang, H.; Liu, R.; Han, Y.; Liu, Y.; Tong, C.; Kang, Z. Carbon Quantum Dots Enhance the Photocatalytic Performance of $BiVO_4$ with Different Exposed Facets. *Dalton Trans.* **2013**, *42*, 6285−6289.
(30) Li, H.; Liu, R.; Liu, Y.; Huang, H.; Yu, H.; Ming, H.; Lian, S.; Lee, S.-T.; Kang, Z. Carbon Quantum Dots/Cu_2O Composites with Protruding Nanostructures and their Highly Efficient (Near) Infrared Photocatalytic Behavior. *J. Mater. Chem.* **2012**, *22*, 17470−17475.
(31) Zhang, H.; Huang, H.; Ming, H.; Li, H.; Zhang, L.; Liu, Y.; Kang, Z. Carbon Quantum Dots/Ag_3PO_4 Complex Photocatalysts with Enhanced Photocatalytic Activity and Stability under Visible Light. *J. Mater. Chem.* **2012**, *22*, 10501−10506.
(32) Merrill, M. D.; Dougherty, R. C. Metal Oxide Catalysts for the Evolution of O_2 from H_2O. *J. Phys. Chem. C* **2008**, *112*, 3655−3666.
(33) Yeo, B. S.; Bell, A. T. In Situ Raman Study of Nickel Oxide and Gold-Supported Nickel Oxide Catalysts for the Electrochemical Evolution of Oxygen. *J. Phys. Chem. C* **2012**, *116*, 8394−8400.
(34) Corrigan, D. A. The Catalysis of the Oxygen Evolution Reaction by Iron Impurities in Thin Film Nickel Oxide Electrodes. *J. Electrochem. Soc.* **1987**, *134*, 377−384.
(35) Khan, A. I.; O'Hare, D. Intercalation Chemistry of Layered Double Hydroxides: Recent Developments and Applications. *J. Mater. Chem.* **2002**, *12*, 3191−3198.
(36) Chou, S.; Cheng, F.; Chen, J. Electrochemical Deposition of $Ni(OH)_2$ and Fe-Doped $Ni(OH)_2$ Tubes. *Eur. J. Inorg. Chem.* **2005**, *2005*, 4035−4039.
(37) Corrigan, D. A.; Knight, S. L. Electrochemical and Spectroscopic Evidence on the Participation of Quadrivalent Nickel in the Nickel Hydroxide Redox Reaction. *J. Electrochem. Soc.* **1989**, *136*, 613−619.
(38) Gorlin, Y.; Jaramillo, T. F. A Bifunctional Nonprecious Metal Catalyst for Oxygen Reduction and Water Oxidation. *J. Am. Chem. Soc.* **2010**, *132*, 13612−13614.
(39) Li, Y.; Hasin, P.; Wu, Y. $Ni_xCo_{3-x}O_4$ Nanowire Arrays for Electrocatalytic Oxygen Evolution. *Adv. Mater.* **2010**, *22*, 1926−1929.
(40) Ming, H.; Ma, Z.; Liu, Y.; Pan, K. M.; Yu, H.; Wang, F.; Kang, Z. H. Large Scale Electrochemical Synthesis of High Quality Carbon Nanodots and their Photocatalytic Property. *Dalton Trans.* **2012**, *41*, 9526−9531.
(41) Paraknowitsch, J. P.; Thomas, A. Doping Carbons Beyond Nitrogen: An Overview of Advanced Heteroatom Doped Carbons with Boron, Sulphur and Phosphorus for Energy Applications. *Energy Environ. Sci.* **2013**, *6*, 2839−2855.
(42) Choi, C. H.; Park, S. H.; Woo, S. I. Binary and Ternary Doping of Nitrogen, Boron, and Phosphorus into Carbon for Enhancing

Electrochemical Oxygen Reduction Activity. *ACS Nano* **2012**, *6*, 7084−7091.